Water Reuse

Water Reuse Vol 12 No 2, 175 doi: 10.2166/wrd.2022.056

Acid-activated bentonite blended with sugarcane bagasse ash as low-cost adsorbents for removal of reactive red 198 dyes

Teshale Adane[a], Sintayehu Mekuria Hailegiorgis[b] and Esayas Alemayehu[c,d,*]

[a] Department of Environmental Engineering, College of Biological and Chemical Engineering, Addis Ababa Science and Technology University, Addis Ababa, P.O. Box 16417, Ethiopia
[b] Bioprocess and Biotechnology Centre of Excellence, Addis Ababa Science and Technology University, Addis Ababa, P.O. Box 16417, Ethiopia
[c] Faculty of Civil and Environmental Engineering, Jimma University, Jimma, P.O. Box 378, Ethiopia
[d] Africa Centre of Excellence for Water Management, Addis Ababa University, Addis Ababa, P.O. Box 1176, Ethiopia
*Corresponding author. E-mail: esayas16@yahoo.com

ABSTRACT

The present research work investigated the removal efficiency of acid-activated bentonite blended with a sugarcane bagasse ash (SCBA) adsorbent for the removal of reactive red 198 (RR198) from a synthetic dye solution. The effect of the adsorption parameters of bentonite on SCBA blending ratio, dye solution pH, adsorption contact, adsorbent dosage, and initial dye concentration was investigated, and the parameters were optimized for maximum RR198 removal from the synthetic dye solution. At an optimum condition of 1:1 bentonite to the SCBA blending ratio, a solution pH of 2, 3.7 g/L of adsorbent dosage, and 15 mg/L of initial dye concentration 150 min of adsorption time, the properties of adsorbents such as adsorbent specific surface area, crystalline phase structure, functional groups, and surface morphologies of the adsorbents were investigated. At optimum conditions, 97% RR198 removal efficiency of the adsorbent was achieved. In order to determine adsorption kinetics and isotherm models, different adsorption models were employed. It was observed that the adsorption of the RR198 dye into the acid-activated bentonite blended with the SCBA adsorbent was represented well by the Langmuir isotherm model and the adsorption kinetics order was found to be the pseudo-second order.

Key words: acid-activated bentonite, batch adsorption processes, reactive red 198 removal, sugarcane bagasse ash

HIGHLIGHTS

- Regenerable and low-cost adsorbents.
- Removal of reactive dye using blended inorganic and organic adsorbents.
- Principle of waste to wealth.
- Improving the quality of industrial wastewater effluents.

GRAPHICAL ABSTRACT

1. INTRODUCTION

Dye-laden wastewater discharge into the environment has created severe environmental problems due to the persistent nature of dyes that significantly affects water bodies. Dyes of synthetic origin have complex structures and most of them are non-biodegradable. Environmental pollution from wastewater containing synthetic-origin dyes, as well as its effect on the ecosystem, has been increasing and has become a serious concern for the general public at all levels (McKay *et al.* 1999; Quan *et al.* 2017). In the industrial sectors such as food, textiles, leather, pharmaceutical, pulp, and paper, thousands of synthetic dyes are being used and discharged into the environment as wastewater. Among the different dye-consuming industries, the textile industry is the major industry that consumes a huge quantity of dyes and different hazardous chemicals that are discharged into the environment and water bodies as wastewater. Different research findings have also reported that discharge from the textile industry has become a matter of serious environmental and health concern for communities and ecosystems in their vicinity (Hameed *et al.* 2009; Carmen & Daniela 2012). Globally, the textile industry consumes about 56% of the total synthetic dyes produced (Jain & Gogate 2018). This figure testifies to the fact that the textile industry is the major consumer of synthetic dyes and discharges a large amount of synthetic dyes containing wastewater. In the textile industry, of all dyes used, from dyeing and finishing process units alone, about 10–25% of dyes are discharged as a by-product or waste product into the surrounding freshwater (Carmen & Daniela 2012).

Of the different types of dyes used in the textile industry, reactive dyes such as RR198 are widely used due to their advantageous properties such as simple application techniques, bright colour, and low energy consumption (Dizge *et al.* 2008). In their research findings, Carmen & Daniel (2012) have reported that the fixation rates of reactive dyes on the surface of materials range from 50 to 90%, while the remaining reactive dyes are discharged into the environment as effluent wastewater. Shoukat *et al.* (2019) have investigated that a dye-laden water body has devastating effects on the photosynthesis of aquatic plants as well as aesthetic value due to the blocking of sunlight. The investigation conducted by Dizge *et al.* (2008) has also demonstrated that dye-containing wastewater has complex molecular structures and high solubility. Due to the synthetic origin of reactive dyes, conventional and biological treatment methods are not effective at meeting the required treatment levels. The mitigation of such hazardous dyes from wastewater has become a matter of urgent importance because of the increasingly alarming environmental threat posed by them, thus attracting the attention of researchers.

Various methods have been investigated and reported for dye removal from water, such as photocatalytic and photochemical processes (Bahadori *et al.* 2020), sedimentation, membrane separation, and flotation (Dharupaneedi *et al.* 2019), electrodialysis (Xue *et al.* 2015), reverse osmosis (Nataraj *et al.* 2009), electrochemical oxidation (Singh *et al.* 2016), advanced oxidation processes (AOPs) like ozonation, and photocatalytic reaction (Somensi *et al.* 2010). Although these methods have their own advantages and disadvantages, their industrial applications are limited. However, the adsorption method is the most commonly used and industrially well-established methods for the removal of dyes from wastewater (Dawood *et al.* 2014). Of the different organic and inorganic adsorbents commercially available, activated carbon (AC) is widely used and is an efficient adsorbent for removing dyes from wastewater as it has better adsorption capacity, a mesoporous and tortuous pore structure, and a large surface area to volume ratio. However, it has the limitation of high production and regeneration cost. Currently, many research studies are being conducted to overcome the limitations posed by commercial-AC. One such option is searching for alternative adsorbents with low cost, better adsorption capacity, and easy availability. Synthesis of adsorbents from agricultural solid wastes such as biomass-based-AC and clay minerals is the best option to achieve the desired objectives. Globally, clay materials have been gaining increased attention as a potential adsorbent due to their low cost, easy accessibility, and easy applicability to industrial scale wastewater treatment (Khataee *et al.* 2015; Li *et al.* 2015). Of the different types of clay, bentonite is a natural clay that is widely available and applied as an adsorbent for the removal of pollutants such as RR198 from wastewater (Amin *et al.* 2015; Toor *et al.* 2015; Belaroussi *et al.* 2018; Javed *et al.* 2018).

Reactive red 198 (RR198), an azo dye group, has been mostly consumed in the textile industry and is one of the major pollutants present in textile wastewater (Salari *et al.* 2021). Various adsorbents have been investigated and reported for the removal of RR198 from textile wastewater. Alumina/carbon nanotubes (Malakootian *et al.* 2015), zeolite modification with cellulose nanofibre/magnetic nanoparticles (Salari *et al.* 2021), and the synthesis of polyaniline/Fe_3O_4 magnetic nanoparticles (Tayebi *et al.* 2016) are among the investigated and reported adsorbents for the removal of RR198 from textile wastewater. However, its large-scale application is limited due to either its long synthesis procedures or their associated high processing cost. In the present research work, efforts have been made to develop adsorbents from low-cost and easily available Ethiopian bentonite for the removal of RR198 from an aqueous solution. The adsorption capacities, chemical

and mechanical stability, and affinity to the adsorbate have been enhanced through acid activation and surface modification with sugarcane bagasse ash (SCBA) for the effective removal of RR198 from the aqueous solution.

2. MATERIALS AND EXPERIMENTAL METHODS

2.1. Materials and chemicals

Bentonite was collected from *Gewane Afar* regional state, and SCBA was collected from *Wonji Shewa* Sugar Factory *Oromia* regional state, Ethiopia, respectively. Both materials were collected and placed in a plastic lining bag and brought to the Addis Ababa Science and Technology University, Environmental Engineering Postgraduate Laboratory (AASTU-EEPL). Sodium hydroxide (NaOH) pellets and hydrochloric acid (HCl, purity >37%) were obtained from AASTU-EEPL. RR198 was obtained from the *Yirgalm Addis* Textile Factory PLC, Ethiopia. RR198 characteristics and its structure are illustrated in Table 1 and Figure 1, respectively. The different apparatuses and equipment used were Brannuer–Emmett–Teller (BET) (SA-9600 series, Japan), X-ray diffraction (XRD) (XRD-7000, Japan), scanning electron microscopy (SEM) (INSPECT, F50, USA) basic shaker (SK-300), Fourier transform infrared spectroscopy (FTIR) (Perkin Elmer, USA), weighing balance, and different types of glassware and lab apparatus.

2.2. Adsorbent and adsorbate preparation

The crushed bentonite was washed using distilled water, dried in an oven (FAITHFUL) adjusted at 105 °C for 12 h, and ground to a powder. The SCBA was also washed using distilled water and dried in an oven set at 105 °C for 12 h. The size reduced and the dried adsorbents were placed in glass bottles for an acid activation experiment. A total of 1,000 mg/L of stock dye solution was prepared using distilled water and diluted as necessary to obtain the dye solution's required inlet concentrations for batch experiments.

2.3. Acid activation adsorbents

The acid activation experiment was carried out in a 250 mL Erlenmeyer flask with a 200-mL working volume at 100 rpm a basic shaker (SK-300) and at 25 °C. Ten grams of prepared bentonite and SCBA for each sample were weighted and added to 0.5–4 M HCl and 23–277 min contact time mixed properly. At the end of the mixing time, the residue was separated from the

Table 1 | Characteristics of RR198

Characteristic	Reactive red 198 (RR198)
Molecular formula	$C_{27}H_{18}C_lN_7Na_4O_{15}S_5$
Colour index name	Reactive Red-198
λ_{max}	520 nm
Class	Monoazo (–N = N-bond)

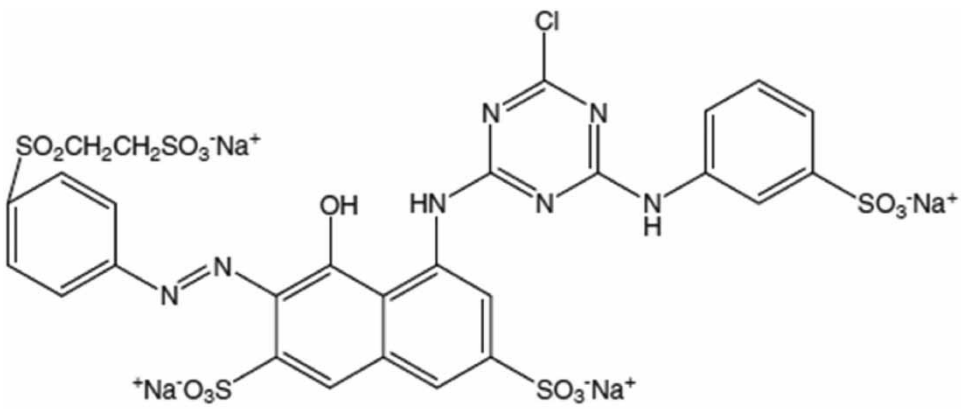

Figure 1 | Chemical structure of RR198 (Alimohammadi *et al.* 2016).

filtrate by using a Buchner funnel. The residual bentonite and SCBA were washed with distilled water several times until they were free from Cl^{-1} ions and pH 5. Then, the samples were dried at 105 °C for 12 h and ground to reach 63 μm with less particle size. Activated adsorbent materials were stored in assigned acid-activated bentonite clay (ABC) and acid-activated sugarcane bagasse ash (ASCBA) in separate glass bottles for further experiments. Based on the specific surface area of the prepared activated adsorbents, the contact time and HCl concentration were selected for further process.

2.4. The point of zero charge (pH_{PZC})

The point of zero charge (pHzpc) is used to explain when the electrical charge of surface adsorbent is zero. The pHpzc for the acid-activated bentonite blended with the acid-activated SCBA used in this study was explained as per the solid addition method described by Aljeboree *et al*. (2017). A known amount of (0.1 g) of acid-activated bentonite blended with acid-activated SCBA was added to 200 mL of 0.1 M of NaCl solution at a pH range of 2–12 adjusted by 0.1 M NaOH or HCl. The blended adsorbents and sodium chloride mixture were placed in a thermoline scientific orbital shaker incubator at a speed of 130 rpm for 24 h. The final solution pH was measured and the pH_{pzc} for each adsorbent was calculated from the pH (initial) vs. ΔpH (initial–final) plot.

2.5. Adsorbent characterization

BET (SA-9600 series, Japan) was used to determine the specific surface of adsorbents before and after activation of the samples. The crystalline phases of adsorbent materials before and after acid activation were identified using XRD (XRD-7000, Japan). SEM (INSPECT, F50, USA) was used to examine the surface morphology of acid-activated and raw adsorbent materials before and after the adsorption of RR198. FTIR (Perkin Elmer, USA) was used for functional group analysis of acid-activated and raw adsorbents. An infrared spectrum was recorded in the region of 4,000–400 cm^{-1} at a resolution of 4 cm^{-1}. A UV spectrophotometer (JASCO V-770, Japan) was used for determining the concentration of RR198 in the solution by recording the UV absorbance at λ_{max} 520 nm.

2.6. Batch adsorption studies

The parametric effects of the adsorbents' blended ratio of 3:1, 1:1, and 1:3; the pH of the solutions from 2 to 12 pH; a contact time of 0–180 min; an initial dye concentration of 15–100 mg/L, and an adsorbent dose of 0.5–3.7 g/L were investigated for a batch adsorption study. The batch experiments were carried out in a 250-mL Erlenmeyer flask with a 200- mL working volume dye solution and the solution was stirred at 200 rpm and at 25 °C. The solution of pH was adjusted by adding 0.1 M NaOH or HCl. After mixing at a given contact time interval, the filtrate was collected for further analysis of the remaining dye concentration in the solution. The absorbance concentration profile was obtained by plotting the calibration curve for RR198 absorbance vs. concentrations graph. The absorbance for each sample was converted using the calibration factor obtained from the calibration curve to calculate the final dye concentration. The amount of dye adsorbed on the adsorbent surface at a given time (t) can be calculated from the mass balance Equation (1).

$$q_t = (C_0 - C_t)\frac{V}{m} \tag{1}$$

where q_t is the amount of dye adsorbed per unit mass of adsorbent (mg/g), C_0 is the initial dye concentration (mg/L), C_t is the equilibrium dye concentration (mg/L), V is the dye solution volume (mL), and m is the adsorbent mass (g).

The percentage of dye removal (%) was evaluated using Equation (2).

$$\text{Percentage of dye removal (\%)} = \frac{(C_0 - C_t)}{C_0} * 100 \tag{2}$$

2.7. Kinetic study

An adsorption kinetic study evaluates the rate or speed of pollutants adsorbed toward the surface from the solution. Therefore, many researchers have applied different kinetic models such as pseudo-first order (PFO, Equation (3)), pseudo-second order (PSO, Equation (4)), and intra-particle diffusion (ID, Equation (5)) models, and these have been commonly used for the adsorption kinetic study (Table 2). The obtained experimental results in this study for RR198 dye removal using acid-activated bentonite blended with SCBA were evaluated by using the aforementioned different kinetic equations shown in Table 2.

Table 2 | PFO, PSO, and ID kinetic models

Models	Equation	References	Equation number
Pseudo-first order	$\log(q_e - q_t) = \log(q_e) - \frac{K_1 t}{2.303}$	Singh *et al.* (2020)	(3)
Pseudo-second order	$\frac{t}{q_t} = \left(\frac{1}{q_e}\right)t + \frac{1}{K_2 q_e^2}$	Singh *et al.* (2020)	(4)
Intra-particle diffusion	$q_t = K_p t^{0.5}$	Alemayehu *et al.* (2011)	(5)

q_e is the mass of dye adsorbed at equilibrium (mg/g), q_t is the mass of dye adsorbed at time t (mg/g), K_1 is PFO constant (min^{-1}), K_2 is PSO constant (g/mg/min), and K_p is ID constant ($mg/g/min^{0.5}$).

2.8. Adsorption isotherms

The Langmuir and Freundlich adsorption isotherm models were used to analyse the interaction between adsorbents and adsorbate molecules at equilibrium. The mathematical expressions of the Langmuir and Freundlich models are expressed in Equations (6) and (7), respectively. The assumption of the Langmuir isotherm model is used to establish the relationship in the monolayer coverage of adsorbate molecules, and those homogeneous active sites exist at the surface of an adsorbent, with no interactions between two adsorbed species (Dehvari *et al.* 2017).

$$\frac{1}{q_e} = \frac{1}{q_{\max} K_L C_e} + \frac{1}{q_{\max}} \tag{6}$$

where q_e (mg/g) is the specific amount of dye adsorbed, and C_e (mg/L) is the dye concentration in the liquid phase at equilibrium.

The Langmuir parameters are $q_{\max}$ (mg/g), which are related to the adsorption density, and K_L (L/mg), which is indicative of the adsorption energy. Both parameters were calculated from the plot $1/q_e$ vs. $1/C_e$.

The assumption the Freundlich isotherm model undergoes adsorption onto the heterogeneous adsorbent. For adsorbate adsorption from solution, the Freundlich isotherm model is described by using Equation (7)

$$\ln q_e = \ln K_f + \frac{1}{n} \ln C_e \tag{7}$$

where q_e (mg/g) is the specific amount of dye adsorbed, and C_e (mg/L) is the dye concentration in the liquid phase at equilibrium.

The parameter K_f (L/g) and n (dimensionless) are the Freundlich constants, which are related to the total adsorption capacity and intensity of adsorption, respectively. The Freundlich constant K_f is used to evaluate the relative capacity or power of adsorption for an adsorbent.

2.9. Desorption study

A desorption study was done to enable adsorbent recycling and reuse several times for the removal of pollutants from wastewater. This activity will reduce the costs of adsorbent and solid wastes (Muralikrishnan & Jodhi 2020). Before the desorption experiments, 3 g/L of acid-activated bentonite blended with SCBA was added to a 250- mL flask containing 200- mL of 30 mg RR198/L solution at a pH of 2 and 25 °C. The flask was shaken at 200 rpm for 120 min until adsorption reached equilibrium and the residual dye concentration determined. The separated residue was added to a 250 mL flask containing 100 mL of 1 M NaOH and that flask was shaken at 100 rpm for 7 h. Desorption capacity (q_e) and efficiency (Q) were calculated using Equations (8) and (9).

$$q_e = V\left(\frac{C_f}{M}\right) \tag{8}$$

where q_e is the amount desorbed (mg/g), V is the solvent solution volume (L), M is the weight of the spent adsorbent (g), and C_f is the dye concentration in the desorbing solution (mg/L).

$$Q(\%) = \left(\frac{q_{e,\text{desorption}}}{q_{e,\text{sorption}}}\right) * 100 \tag{9}$$

3. RESULTS AND DISCUSSION

3.1. Adsorbent characterization

3.1.1. Crystalline structures

The XRD results for bentonite and SCBA are shown in Figure 2(a)–2(d). Figure 2(c) and 2(b) show strong peaks at $2\theta =$ 19.75°, 26.65°, and 28° for raw bentonite and 19.9°, 20.98°, and 26.8° for acid-activated bentonite. XRD analysis of raw and acid-activated bentonite indicates the presence of quartz as the main component. Gypsum, cristobalite, and quartz are also present (Ajemba 2014). Similar results were reported by investigators (Zhao *et al.* 2010; Khalilzadeh Shirazi *et al.* 2020) for raw bentonite clay at $2\theta = 26.68°$, 28.59°, and 36.11°. On the other hand, strong peaks at $2\theta = 24.6°$, 26.7°, 28°, and 35.6° for raw SCBA and 21.9°, 26.6°, 27.7°, and 36.8° for acid-activated SCBA were obtained (Figure 2(a) and 2(d)), respectively. As can be predicted, SCBA has quartz as the main component. A similar result was reported by Alves *et al.* (2017) for raw SCBA. In general, all four samples showed approximately similar patterns, demonstrating that the activating processes did not have a significant effect on the structure of the adsorbents.

3.1.2. SEM analysis

The surface morphology of the adsorbents before and after adsorption process is shown in Figure 3(a)–3(e). The SEM images in Figure 3(a) and 3(c) show that the surface of raw bentonite and SCBA is rough and uneven. However, after acid activation (Figure 3(b) and 3(d)), the adsorbents' surface of both adsorbents became rougher, dense, high pores, with available active sites, and the internal surface. These changes in the morphological properties of adsorbents are due to the removal of impurities from bentonite and the SCBA surface. As can be seen from Figure 3(b) and 3(d), more irregular and significant numbers of pores due to the modification of adsorbents were observed, which indicate more dye molecules on the surface adsorbed. In Figure 3(e), a smaller proportion of irregular structures, including active sites and pores, were also observed, which may be elucidated by the slight reduction in particle structure of the adsorbents during the modification and adsorption processes. Similar remarks about porous structure improvement and adsorption for surface modification of the SCBE (Faria *et al.* 2012; Alves *et al.* 2017; Farirai *et al.* 2020) and raw bentonite (Javed *et al.* 2018) were also reported.

3.1.3. FTIR analysis

The FTIR results for all adsorbents are shown in Figure 4(a)–4(d). The raw bentonite absorption band at 3,600 and 1,639 cm^{-1} indicates O–H group bending and stretching in hydration water on the bentonite surface. A similar study was reported by Al-Essa (2018). An absorption band at 1,027 cm^{-1} is recognized for stretching vibration Si–O bands, which is strong evidence for a silicate structure. The band at 796 cm^{-1} confirmed the presence of quartz in the raw bentonite as reported by Zhirong *et al.* (2011). The activated bentonite absorption band at 3,621 cm^{-1} shows a free O–H group on the surface of the activated bentonite. A peak was also observed at 1,626 cm^{-1} bending and stretching bands Al – Al-OH, which indicates a leaching out of octahedral cations like Al^{3+} and Mg^{2+} from the structure of bentonite. The peak observed at 1,001 cm^{-1} shows the

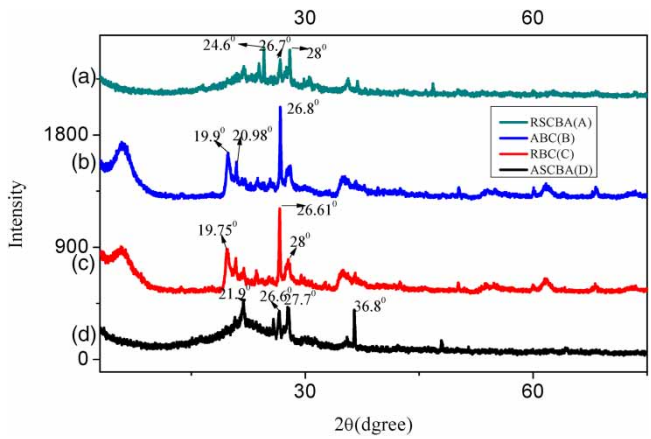

Figure 2 | (a–d) XRD results of RSCBA (a), ABC (b), RBC (c), and ASCBA (d).

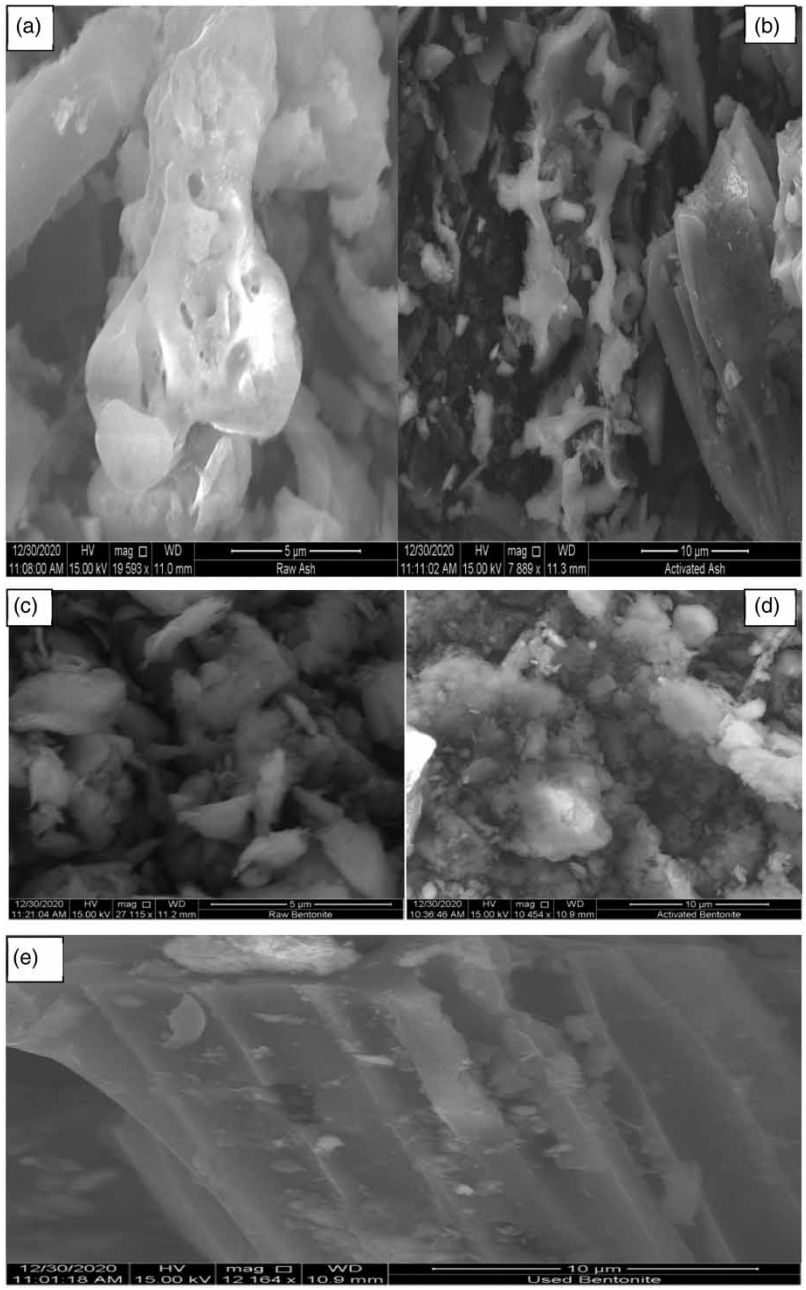

Figure 3 | SEM image of raw SCBA (a), activated SCBA (b), raw bentonite (c), activated bentonite (d), and (e) mixed activated bentonite and SCBA after dye adsorption.

availability of amorphous silica on activated bentonite. A previous study (Bendou & Amrani 2014) also reported that modified bentonite is rich in amorphous silica.

On the other hand, the FTIR analysis of raw SCBA shows a peak at 2,988 cm^{-1} representing the presence of O–H on the raw ash surface. The FTIR analysis of acid-activated SCBA shows a peak at 2,982 cm^{-1} indicating the presence of the O–H group on the surface of activated ash. The peak observed at 1,049 and 1,053 cm^{-1} is attributed to Si–O–Si symmetric and asymmetric stretching on acid-activated and raw SCBA, respectively. According to a previous investigation, the bands observed at about 450–455 and 1,050–1,070 cm^{-1} were attributed to the Si–O–Si symmetric and asymmetric stretching, respectively (Kalapathy *et al.* 2000; Mourhly *et al.* 2015). The presence of a band at approximately 770–797 cm^{-1} is due to the Si–O–Si symmetric stretching as reported by Rahman *et al.* (2015). In general, it can be observed that most band

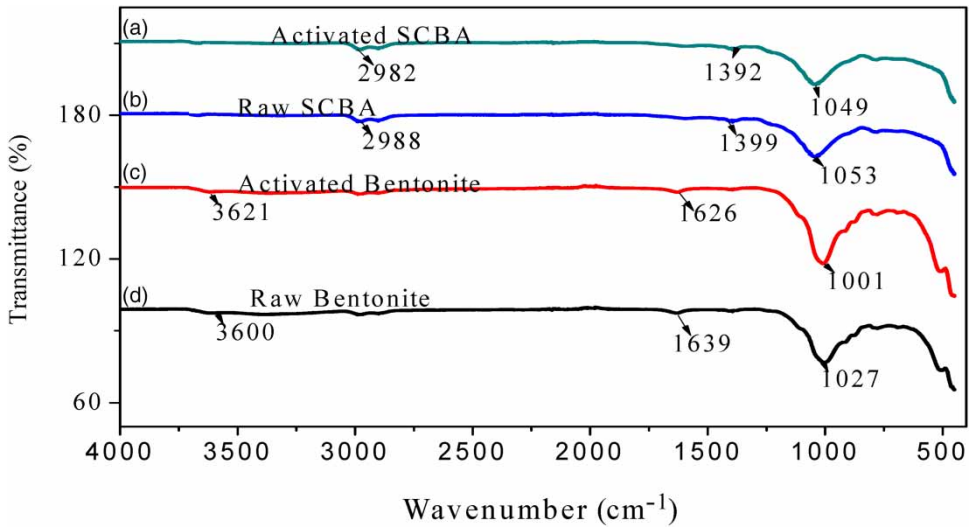

Figure 4 | FTIR results of acid-activated SCBA (a), raw SCBA (b), activated bentonite (c), and raw bentonite (d).

positions have not changed during the surface modification processes, which implies that the basic adsorbent's structure has not collapsed.

3.1.4. BET analysis

The specific surface area of the adsorbents was measured using a nitrogen gas adsorption–desorption technique at 77 k using the surface analyser equipment (SA-9600 series, Japan). The specific surface areas (BET values) of the adsorbents were compared. Accordingly, 57.7, 100.97, 4.94, and 30.85 m^2/g of raw bentonite, acid-activated bentonite, raw SCBA, and acid-activated SCBA were evaluated, respectively. It was observed that activating with acid enhanced the specific surface area of the adsorbents. Similar observations have been reported for raw bentonite 13.9 m^2/g (Carvalho *et al.* 2019), 12 m^2/g (Santos *et al.* 2016), 66.2 m^2/g (Al-Essa 2018), and 25.7 m^2/g (Toor *et al.* 2015), for acid-activated bentonite 287.8 m^2/g (Al-Essa 2018) and 84.12 m^2/g (Toor *et al.* 2015), and for raw SCBA 1.5 m^2/g (Farirai *et al.* 2020).

3.2. The point of zero charge (pH_{pzc})

The pH_{pzc} for acid-activated bentonite blended with acid-activated SCBA was found to be 5.6 (Figure 5). When the solution pH is less than the pH_{pzc} of the adsorbent, more positive charge density is expected to bind on the surface of the adsorbent, hence increasing the removal efficiency of anionic dyes. As expected, when the pH was lower than the pH_{pzc}, RR198 was highly adsorbed onto the surface of the adsorbent due to columbic attraction. A similar observation was reported for AC prepared from wastes (Acevedo *et al.* 2015).

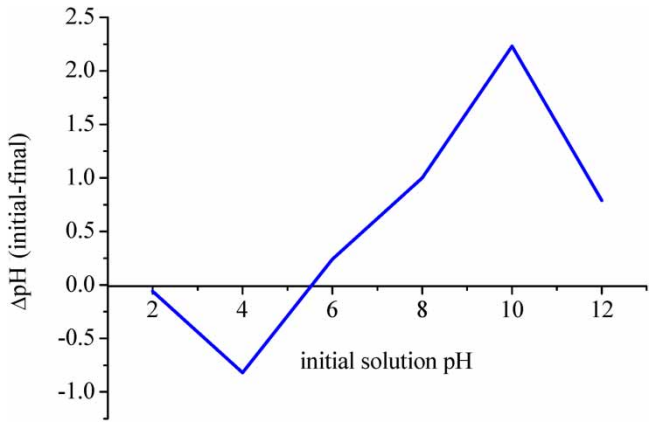

Figure 5 | Point zero charge (pH_{pzc}) of mixed acid-activated bentonite and acid-activated SCBA.

3.3. Effect of adsorbent blended ratio

In this investigation, batch experiments were carried out at different acid-activated adsorbent blended ratios at 25 °C and 200 rpm. Table 3 shows the effect of ABC blended with ASCBA on the adsorption of RR198, while other parameters such as an initial concentration of 70 mg/L, a contact time of 60 min, and an adsorbent dose of 2.5 g/L were kept constant. As can be seen in Table 3, the proportional dye removal increased when the blended ratio of the adsorbents was one to one (1:1). This might be attributed to the fact that both adsorbents have adequate active sites for the adsorption of RR198. Preliminary studies also confirmed that the RR198 removal efficiency of the single (unblended) adsorbent was lower than that of the blended one; i.e. the activated SCBA was 58% and activated bentonite was 82% (data not given). Hence, activated bentonite blended with SCBA was chosen in this study. Additional testing of the individual adsorbents, including their removal mechanisms, is, however, required to verify whether the removal of RR198 using a blended adsorbent is a sustainable method.

3.4. Effect of pH

Elimination of dyes from water depends on the pH of the solution (Kausar & Bhatti 2013), since pH can change the adsorbents' and pollutants' interaction surface charge, which enhances repulsion or attraction (Kausar *et al.* 2018). In this investigation, the batch experiments were carried out at different solution pH values of 2, 4, 6, 8, 10, and 12, while other parameters such as initial dye concentration (30 mg/L), contact time (60 min), and adsorbent dose (2 g/L) were kept constant at 25 °C and 200 rpm. As can be observed in Figure 6, the percentage of RR198 removed from the aqueous solution significantly decreases (from 97 to 3.3%) as the pH of the solution increases from 2 to 12, indicating that the adsorption of RR198 is likely to be based on physical interactions between the surface of the adsorbent and the adsorbate (Salari *et al.* 2021). At the lower pH range, adsorption increases due to increasing protonation (Alimohammadi *et al.* 2016). At high pH values, the competition with OH ions increases, and RR198 adsorption decreases. Similar reports confirm that RR198 removal is less efficient under alkaline conditions (Rashid *et al.* 2016; Naeem *et al.* 2017).

Table 3 | Effect of various blended ratios (operative conditions – C_0: 70 mg/L; time: 60 min; adsorbent dose: 2.5 g/L)

Blended ratio (ASCBA:ABC)	Proportional dye removal (%)
1:3	85
1:1	97
3:1	75

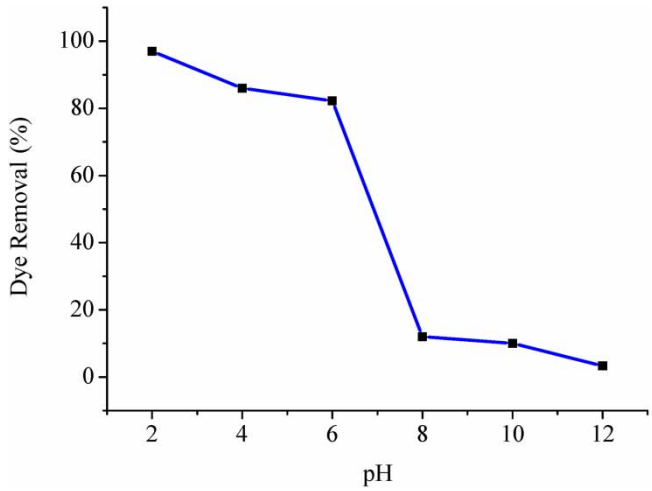

Figure 6 | Effect of pH on RR198 dye removal efficiency (operative conditions – C_0: 30 mg/L; time: 60 min; adsorbent dose: 2 g/L).

3.5. Effect of contact time

A further, similar set-up of batch studies were carried out with various contact times (0, 30, 60, 90, 120, 150, and 180 min). All other parameters were kept constant, such as the adsorbent blended ratio (1:1), initial dye concentration (30 mg/L), solution of pH (2 pH), and adsorbent dose (3.7 g/L). Figure 7 shows that dye removal begins at some points within 30 min and then continues at a constant rate until almost reaching equilibrium after 150 min. According to the experimental results, the highest dye removal efficiency was achieved at a contact time of 150 min. The increased contact time enhanced the interaction between dye molecule and the adsorbent.

When the contact time increases, dye removal also initially increases and finally becomes a constant trend, illustrating attained equilibrium. The initial adsorption of dye is fast due to the availability of vacant active sites on the surface of the adsorbent which can be occupied easily by the RR198 dye because a phenomenal, high removal efficiency was achieved (Mollahosseini *et al.* 2019). After a certain time, only too low increments in the dye removal were observed because there were few active sites on the surface adsorbent. After a 150 min removal, no change in efficiency was observed. Thus, an optimal contact time of 150 min was selected for the other experiments.

3.6. Effect of initial dye concentration

The effect of the initial RR198 concentration that varied in the range of 15–100 mg/L on the adsorption was investigated under specific conditions (a contact time of 150 min; adsorbent dose of 3.7 g/L; pH of 2; blended ratio of 1:1; at 25 °C). The RR198 adsorption efficiencies and calculated adsorption densities depending on the initial concentration are shown in Figure 8. In the processes, the concentrations of the dye play an important role. On changing the initial concentration of the RR198 solution from 15 to 100 mg/L, the adsorption densities increase from 0.79 to 3.8 mg of RR198 per gram of the adsorbent. On the other hand, with a lower initial concentration of RR198, the adsorption efficiency (percentage removal) is higher than the efficiency attained when higher initial concentrations are used (Figure 8). While the RR198 adsorption yield was found as 97.2% for 15 mg/L of the initial concentration, this value was 65.7% for that of 100 mg/L. These results indicate that the competition for adsorption sites becomes rigorous, and energetically less favourable sites become involved with increasing RR198 concentrations in the solution. This is a common finding and has been largely reported in the literature (Zhou *et al.* 2019; Mirzapour *et al.* 2020).

3.7. Effect of adsorbent dosage

A series of batch experiments were carried out using various adsorbent doses of 0.5, 1, 1.5, 2.5, 3, and 3.7 g/L, while the other parameters were kept constant, such as initial dye concentration (70 mg/L), contact time (60 min), and solution pH (2 pH) at 25 °C. By changing the dose from 0.5 to 3.7 g/L, the removal efficiency of RR198 increased from 81.4 to 94% (Figure 9). The maximum removal efficiency was exhibited at 3.7 g/L of the adsorbent. This observation was attributed to the increase in the number of free adsorption sites. However, RR198 adsorbed per unit mass of the adsorbent significantly decreased with an increasing adsorbent dose (from 22.8 to 4.4 mg/g). This may be attributed to the higher adsorbent amount creating particle

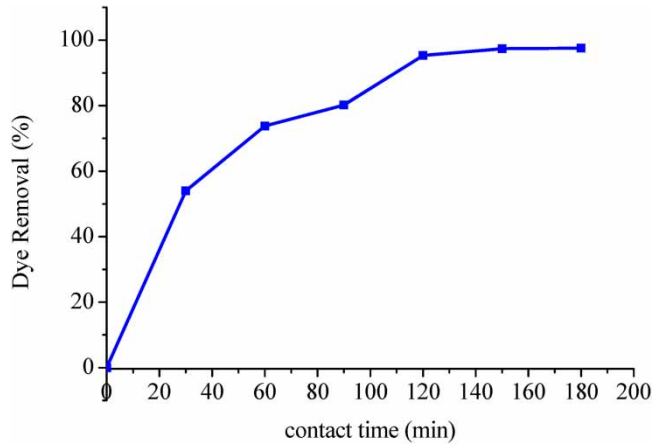

Figure 7 | Effect of contact time (operative conditions – C_0: 30 mg/L; pH: 2; adsorbent dose: 3.7 g/L; adsorbent blended ratio: 1:1).

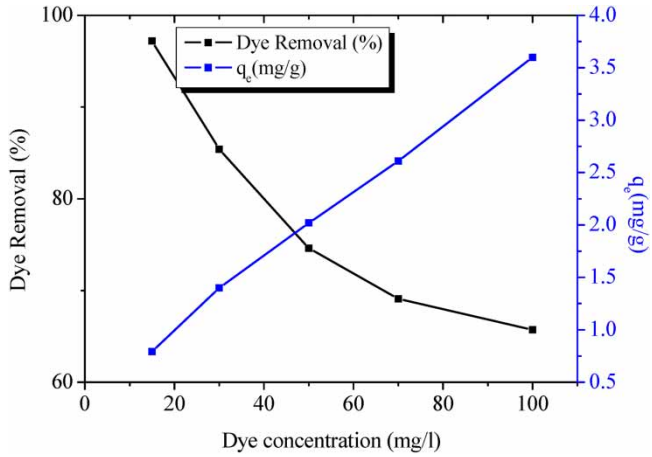

Figure 8 | Effect of initial dye concentration (operative conditions – contact time: 150 min; pH: 2; adsorbent dose: 3.7 g/L; blended ratio: 1:1).

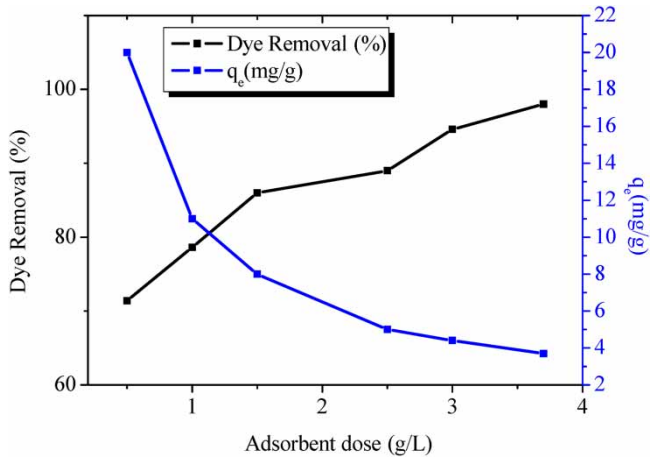

Figure 9 | Effect of adsorbent dosage (operative conditions – contact time: 60 min; pH: 2; C_0: 70 mg/L; adsorbent dose: 3.7 g/L).

aggregation, resulting in a decrease in the total surface area and an increase in diffusional path length, both of which contribute to a decrease in the amount adsorbed per unit mass (Figure 9). These observations were also confirmed by other investigators (Elkady *et al.* 2011; Ghaneian *et al.* 2015; Bellifa *et al.* 2017; Dehvari *et al.* 2017).

3.8. Adsorption kinetics modelling

In order to define the kinetics of RR198 adsorption, the parameters for the adsorption process were studied for the contact time ranging between 30 and 180 min by monitoring the present removal of RR198 by the adsorbent. The equilibrium parameters $q_{e(\exp)}$ and $q_{e(\mathrm{cal})}$ (mg/g) and the adsorption rate constant K_1 (min^{-1}) and K_2 (g/mg/h) are reported in Table 4. The kinetic plots were prepared (data not given). The calculated equilibrium capacity values ($q_{e(\mathrm{cal})}$) were very close to the experimentally determined values ($q_{e(\exp)}$). Excellent fits ($R^2 = 0.992$) indicated that the PSO kinetic model was applicable. The applicability of this model implies that the rate-limiting step may be chemisorption involving valence forces through sharing or exchanging of electrons between the adsorbent and the adsorbate. Although the adsorption process in the present experiment is considered as a surface phenomenon, it is also postulated that the rate-limiting step in the adsorption process might include intra-particle diffusion. As expected, the plots of q_t vs. $t^{0.5}$, according to the intra-particle diffusion model (Equation (5)), were linear (data not given), and the related parameters are listed in Table 4. K_p is the characteristic for the rate of adsorption, where intra-particle diffusion is rate controlling in nature. Similar trends were reported by other investigators (Tayebi *et al.* 2016; Mirzapour *et al.* 2020).

Table 4 | Parameters obtained from PFO, PSO, and ID models (operating conditions – contact time: 150 min; C_0: 50 mg/L)

PFO				PSO				ID	
$q_{e(cal)}$ (mg/g)	$q_{e(exp)}$ (mg/g)	K_1 (min^{-1})	R^2	$q_{e(cal)}$ (mg/g)	$q_{e(exp)}$ (mg/g)	K_2 (g/mg/min)	R^2	K_p (mg/g/$min^{0.5}$)	R^2
2.4	2.63	0.022	0.874	2.58	2.63	0.036	0.992	0.184	0.85

3.9. Adsorption isotherms

The adsorption of RR198 onto the adsorbent was described by both Freundlich and Langmuir isotherm models. The Freundlich model assumes that adsorption occurs on a heterogeneous surface through multilayer adsorption, and the adsorbed amount increases with increasing equilibrium concentrations. In contrast, the Langmuir model assumes an asymptotic approach to a monolayer surface coverage (Alemayehu *et al.* 2011). In this work, an analysis of the relationship between the adsorption capacity of the adsorbent and different RR198 initial concentrations (from 15 to 100 mg/L) was performed using isotherm equations (Equations (6) and (7), as given in subsection 2.8). The related parameters for the fitting of both equations at constant temperature are summarized in Table 5. From the obtained optimization procedure, it became evident that the Langmuir isotherm equation ($R^2 = 0.98$) described the system better than the Freundlich isotherm equation ($R^2 = 0.86$). This indicated the homogeneous distribution of binding sites on the surface of the mixed adsorbents, which had no interaction of dye molecules.

The blended adsorbent sorption isotherms utilized in this work was also compared with previously studied adsorbents for the uptake of dyes, as shown in Table 6. As can be seen in the table, the RR198 uptake capacity of the blended adsorbent used in this study is higher than the AC/bentonite/Fe_3O_4 blended adsorbent (Mirzapour *et al.* 2020). Above all, the raw materials (bentonite and SCBA) are easily accessible and readily available, in contrast to some of the other adsorbents, confirming that acid-activated bentonite blended with SCBA could be a promising candidate for the uptake of RR198 from wastewater.

Table 5 | Isotherm models for RR198 adsorption onto acid-activated bentonite blended with SCBA

Langmuir			Freundlich		
q_{max} (mg/g)	K_L (L/mg)	R^2	K_f (L/g)	1/*n*	R^2
14.67	53.74	0.98	2.66	0.69	0.86

Table 6 | Dye adsorption capacity of various adsorbents

Dyes	Adsorbents	Adsorption capacity (mg/g)	Isotherm models	References
Reactive red 198	PAni/Fe_3O_4 magnetic nanoparticles	45.454	Langmuir	Tayebi *et al.* (2016)
Basic violet 16 (BV16) and reactive red 195	Natural bentonite and charred dolomite	821.63 and 7.03	Langmuir	Khalilzadeh *et al.* (2020)
Reactive black 5	Chemically modified banana peel powder	211.8	Langmuir	Munagapati *et al.* (2020)
Reactive black 5 and Congo red	Banana peel powder	49.2 and 164.6	Langmuir	Subbaiah *et al.* (2018)
Acid blue 25	Phosphoric acid treated rubber leaf powder	28.09	Langmuir	Khalid *et al.* (2015)
Reactive red 198	Activated carbon/bentonite/Fe_3O_4 nanocomposite	4.86	Langmuir	Mirzapour *et al.* (2020)
Reactive dyes red 198	Acid-activated bentonite blended with SCBA	14.67	Langmuir	This study
Reactive red 141	Activated carbon	41.5	Freundlich	Leechart *et al.* (2009)

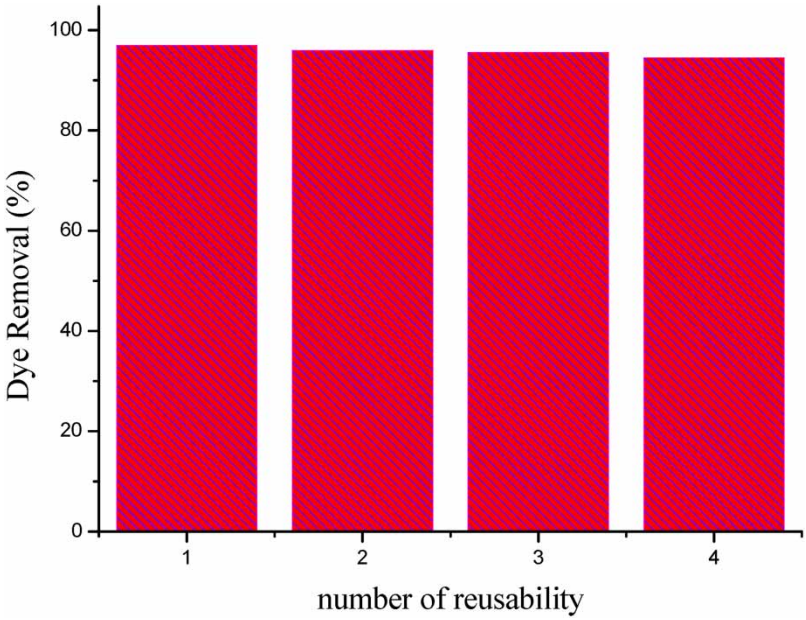

Figure 10 | Number of reusability vs. proportional dye removal.

3.10. Desorption and reusability test

To develop a cost-effective adsorbent for pollutant removal from an aqueous environment, it is important that the adsorbent should be regenerated for reuse. The pH effect on the efficiency of RR198 adsorption on the blended adsorbent showed (Figure 6) that RR198 adsorption capacity was very low at pH >8, suggesting the possibility of desorbing adsorbed RR198 from the saturated adsorbent using an alkaline solution. Based on this, batch desorption–adsorption experiments were carried out as explained in subsection 2.9. The RR198-loaded adsorbent was successfully regenerated using an alkaline solution. Figure 10 shows the blended adsorbent's removal efficiency through four cycles of the desorption–adsorption process. As can be observed in the desorption and reusability experiments, the adsorption capacities of the regenerated adsorbents were found to be effective (94.5%) to remove RR198 from aqueous solutions. Hence, these results confirmed that acid-activated bentonite blended with SCBA can be reused several times for RR198 removal from wastewater, implying that it is found to be a promising material.

4. CONCLUSION

RR198 adsorption was tested using acid-activated bentonite blended with SCBA as the adsorbent. Adsorption parameters were applied to describe the best removal performance. The maximum removal efficiency (97%) was attained at optimal parameters such as an adsorbent blended ratio of 1:1, a solution pH of 2, a contact time of 150 min, an adsorbent dose of 3.7 g/L, and an initial dye concentration of 15 mg/L. The adsorption isotherm model was fitted better by Langmuir than by Freundlich, and the PSO model fitted the adsorption kinetics better than the other models. The RR198-loaded adsorbent was successfully regenerated using an alkaline solution. Therefore, the results of the study demonstrated that a low-cost acid-activated blended adsorbent could be considered as a promising material for the removal of dyes from wastewater. Additional testing of the blended adsorbent in a continuous reactor is, however, required to verify whether the removal of RR198 from dye-laden industrial wastewater is more efficient.

ACKNOWLEDGEMENTS

We would like to thank the Addis Ababa Science and Technology University, Environmental Engineering Department, for offering us full laboratory facilities, the *Yirgalem Addis* Textile Factory for providing reactive dyes, the *Wonji Shewa* Sugar Factory for providing SCBA, and the Candela Pharmaceutical Industry for providing an FTIR instrument for the analysis of samples.

FUNDING

This work was supported by the Addis Ababa Science and Technology University and the *Debre Tabor* University.

DATA AVAILABILITY STATEMENT

All relevant data are included in the paper or its Supplementary Information.

REFERENCES

Acevedo, B., Rocha, R. P., Pereira, M. F. R., Figueiredo, J. L. & Barriocanal, C. 2015 Adsorption of dyes by ACs prepared from waste tyre reinforcing fibre. Effect of texture, surface chemistry and pH. *Journal of Colloid and Interface Science* **459**, 189–198.

Ajemba, R. O. 2014 Modification of Ntezi bentonite structure by hydrochloric acid: process kinetics and structural properties of the modified samples. *Pakistan Journal of Scientific and Industrial Research Series A: Physical Sciences* **57** (1), 1–9.

Alemayehu, E., Thiele-Bruhn, S. & Lennartz, B. 2011 Adsorption behaviour of Cr(VI) onto macro and micro-vesicular volcanic rocks from water. *Separation and Purification Technology* **78** (1), 55–61.

Al-Essa, K. 2018 Activation of Jordanian bentonite by hydrochloric acid and its potential for olive mill wastewater enhanced treatment. *Journal of Chemistry* **2018**. https://doi.org/10.1155/2018/8385692.

Alimohammadi, Z., Younesi, H. & Bahramifar, N. 2016 Batch and column adsorption of reactive red 198 from textile industry effluent by microporous activated carbon developed from walnut shells. *Waste and Biomass Valorization* **7** (5), 1255–1270.

Aljeboree, A. M., Alshirifi, A. N. & Alkaim, A. F. 2017 Kinetics and equilibrium study for the adsorption of textile dyes on coconut shell activated carbon. *Arabian Journal of Chemistry* **10**, S3381–S3393.

Alves, R. H., Reis, T. V. D. S., Rovani, S. & Fungaro, D. A. 2017 Green synthesis and characterization of biosilica produced from sugarcane waste ash. *Journal of Chemistry* **2017**. https://doi.org/10.1155/2017/6129035.

Amin, M. T., Alazba, A. A. & Shafiq, M. 2015 Adsorptive removal of reactive black 5 from wastewater using bentonite clay: isotherms, kinetics and thermodynamics. *Sustainability (Switzerland)* **7** (11), 15302–15318.

Bahadori, E., Rapf, M., Di Michele, A. & Rossetti, I. 2020 Photochemical vs. photocatalytic azo-dye removal in a pilot free-surface reactor: is the catalyst effective? *Separation and Purification Technology* **237**, 116320.

Belaroussi, A., Labed, F., Khenifi, A., Akbour, R. A., Bouberka, Z., Kameche, M. & Derriche, Z. 2018 A novel approach for removing an industrial dye 4GL by an Algerian bentonite. *Acta Ecologica Sinica* **38** (2), 148–156.

Bellifa, A., Makhlouf, M. & Boumila, Z. H. 2017 Comparative study of the adsorption of methyl orange by bentonite and activated carbon. *Acta Physica Polonica A* **132** (3), 466–468.

Bendou, S. & Amrani, M. 2014 Effect of hydrochloric acid on the structural of sodic-bentonite clay. *Journal of Minerals and Materials Characterization and Engineering* **02** (05), 404–413.

Carmen, Z. & Daniel, S. 2012 Textile organic dyes - characteristics, polluting effects and separation/elimination procedures from industrial effluents - a critical overview. In: Puzyn, T & Aleksandra Mostrag-Szlichtyng, A (eds). *Organic Pollutants Ten Years after the Stockholm Convention - Environmental and Analytical Update*. IntechOpen, London. 484 p. 10.5772/1381

Carvalho, L. A. S. J., Konzen, R. A., Cunha, A. C. M., Batista, P. R., Bassetti, F. J. & Coral, L. A. 2019 Efficiency of activated carbons and natural bentonite to remove direct orange 39 from water. *Journal of Environmental Chemical Engineering* **7** (6), 103496.

Dawood, S., Sen, T. K. & Phan, C. 2014 Synthesis and characterisation of novel-activated carbon from waste biomass pine cone and its application in the removal of Congo red dye from aqueous solution by adsorption. *Water, Air, and Soil Pollution* **225**, 1818.

Dehvari, M., Ehrampoush, M. H., Ghaneian, M. T., Jamshidi, B. & Tabatabaee, M. 2017 Adsorption kinetics and equilibrium studies of reactive red 198 dye by cuttlefish bone powder. *Iranian Journal of Chemistry and Chemical Engineering* **36** (2), 143–151.

Dharupaneedi, S. P., Nataraj, S. K., Nadagouda, M., Reddy, K. R., Shukla, S. S. & Aminabhavi, T. M. 2019 Membrane-based separation of potential emerging pollutants. *Separation and Purification Technology* **210**, 850–866.

Dizge, N., Aydiner, C., Demirbas, E., Kobya, M. & Kara, S. 2008 Adsorption of reactive dyes from aqueous solutions by fly ash: kinetic and equilibrium studies. *Journal of Hazardous Materials* **150** (3), 737–746.

Elkady, M. F., Ibrahim, A. M. & El-Latif, M. M. A. 2011 Assessment of the adsorption kinetics, equilibrium and thermodynamic for the potential removal of reactive red dye using eggshell biocomposite beads. *Desalination* **278** (1–3), 412–423.

Faria, K. C. P., Gurgel, R. F. & Holanda, J. N. F. 2012 Recycling of sugarcane bagasse ash waste in the production of clay bricks. *Journal of Environmental Management* **101**, 7–12.

Farirai, F., Mupa, M. & Daramola, M. O. 2020 An improved method for the production of high purity silica from sugarcane bagasse ash obtained from a bioethanol plant boiler. *Particulate Science and Technology*, 1–8.

Ghaneian, M. T., Jamshidi, B., Dehvari, M. & Amrollahi, M. 2015 Pomegranate seed powder as a new biosorbent of reactive red 198 dye from aqueous solutions: adsorption equilibrium and kinetic studies. *Research on Chemical Intermediates* **41** (5), 3223–3234.

Hameed, B. H., Ahmad, A. A. & Aziz, N. 2009 Adsorption of reactive dye on palm-oil industry waste: equilibrium, kinetic and thermodynamic studies. *Desalination* **247** (1–3), 551–560.

Jain, S. N. & Gogate, P. R. 2018 Efficient removal of Acid Green 25 dye from wastewater using activated *Prunus dulcis* as biosorbent: batch and column studies. *Journal of Environmental Management* **210**, 226–238.

Javed, S. H., Zahir, A., Khan, A., Afzal, S. & Mansha, M. 2018 Adsorption of mordant Red 73 dye on acid activated bentonite: kinetics and thermodynamic study. *Journal of Molecular Liquids* **254**, 398–405.

Kalapathy, U., Proctor, A. & Shultz, J. 2000 A simple method for production of pure silica from rice hull ash. *Bioresource Technology* **73**, 257–262.

Kausar, A. & Bhatti, H. N. 2013 Adsorptive removal of uranium from wastewater: a review. *Journal of the Chemical Society of Pakistan* **35** (3), 1041–1052.

Kausar, A., Iqbal, M., Javed, A., Aftab, K., Nazli, Z., Nawaz, H. & Nouren, S. 2018 Dyes adsorption using clay and modified clay: a review. *Journal of Molecular Liquids* **256**, 395–407.

Khalid, K., Ngah, W. S., AKM Hanafiah, M., Malek, N. S., Khazaai, S. N. & Pahang Malaysia, M. 2015 Acid blue 25 adsorption onto phosphoric acid treated rubber leaf powder. *American Journal of Environmental Engineering* **5** (3A), 19–25.

Khalilzadeh, E., Jörg, S., Klaus, W. M., Amir, F. & Hassani, H. 2020 Design and cost analysis of batch adsorber systems for removal of dyes from contaminated groundwater using natural low-cost adsorbents. *International Journal of Industrial Chemistry* **11** (2), 101–110.

Khalilzadeh Shirazi, E., Metzger, J. W., Fischer, K. & Hassani, A. H. 2020 Removal of textile dyes from single and binary component systems by Persian bentonite and a mixed adsorbent of bentonite/charred dolomite. *Colloids and Surfaces A: Physicochemical and Engineering Aspects* **598**, 124807.

Khataee, A., Sheydaei, M., Hassani, A., Taseidifar, M. & Karaca, S. 2015 Sonocatalytic removal of an organic dye using TiO_2/montmorillonite nanocomposite. *Ultrasonics Sonochemistry* **22**, 404–411.

Leechart, P., Nakbanpote, W. & Thiravetyan, P. 2009 Application of 'waste' wood-shaving bottom ash for adsorption of azo reactive dye. *Journal of Environmental Management* **90** (2), 912–920.

Li, C., Zhong, H., Wang, S., Xue, J. & Zhang, Z. 2015 Removal of basic dye (methylene blue) from aqueous solution using zeolite synthesized from electrolytic manganese residue. *Journal of Industrial and Engineering Chemistry* **23**, 344–352.

Malakootian, M., Mansoorian, H. J., Hosseini, A. & Khanjani, N. 2015 Evaluating the efficacy of alumina/carbon nanotube hybrid adsorbents in removing Azo Reactive Red 198 and Blue 19 dyes from aqueous solutions. *Process Safety and Environmental Protection* **96**, 125–137.

McKay, G., Porter, J. F. & Prasad, G. R. 1999 The removal of dye colours from aqueous solutions by adsorption on low-cost materials. *Water, Air, and Soil Pollution* **114** (3–4), 423–438.

Mirzapour, P., Kamyab Moghadas, B., Tamjidi, S. & Esmaeili, H. 2020 Activated carbon/bentonite/Fe_3O_4 nanocomposite for treatment of wastewater containing Reactive Red 198. *Separation Science and Technology (Philadelphia)* **56** (16), 1–15.

Mollahosseini, A., Khadir, A. & Saeidian, J. 2019 Core–shell polypyrrole/Fe_3O_4 nanocomposite as sorbent for magnetic dispersive solid-phase extraction of Al^{+3} ions from solutions: investigation of the operational parameters. *Journal of Water Process Engineering* **29**, 100795.

Mourhly, A., Khachani, M., El Hamidi, A., Kacimi, M., Halim, M. & Arsalane, S. 2015 The synthesis and characterization of low-cost mesoporous silica SiO_2 from local pumice rock. *Nanomaterials and Nanotechnology* **5** (35). Doi: 10.5772/62033.

Munagapati, V. S., Wen, J. C., Pan, C. L., Gutha, Y., Wen, J. H. & Reddy, G. M. 2020 Adsorptive removal of anionic dye (Reactive Black 5) from aqueous solution using chemically modified banana peel powder: kinetic, isotherm, thermodynamic, and reusability studies. *International Journal of Phytoremediation* **22** (3), 267–278.

Muralikrishnan, R. & Jodhi, C. 2020 Biodecolorization of Reactive Dyes Using Biochar Derived from Coconut Shell: Batch, Isotherm, Kinetic and Desorption Studies **16**, 7734–7742.

Naeem, H., Bhatti, H. N., Sadaf, S. & Iqbal, M. 2017 Uranium remediation using modified *Vigna radiata* waste biomass. *Applied Radiation and Isotopes* **123**, 94–101.

Nataraj, S. K., Hosamani, K. M. & Aminabhavi, T. M. 2009 Nanofiltration and reverse osmosis thin film composite membrane module for the removal of dye and salts from the simulated mixtures. *Desalination* **249** (1), 12–17.

Quan, X., Luo, D., Wu, J., Li, R., Cheng, W. & Ge, S. 2017 Ozonation of acid red 18 wastewater using O_3/$Ca(OH)_2$ system in a micro bubble gas-liquid reactor. *Journal of Environmental Chemical Engineering* **5** (1), 283–291.

Rahman, N. A., Widhiana, I., Juliastuti, S. R. & Setyawan, H. 2015 Colloids and surfaces A: physicochemical and engineering aspects synthesis of mesoporous silica with controlled pore structure from bagasse ash as a silica source. *Colloids and Surfaces A: Physicochemical and Engineering Aspects* **476**, 1–7.

Rashid, A., Bhatti, H. N., Iqbal, M. & Noreen, S. 2016 Fungal biomass composite with bentonite efficiency for nickel and zinc adsorption: a mechanistic study. *Ecological Engineering* **91**, 459–471.

Salari, N., M.A. Tehrani, R. & Motamedi, M. 2021 Zeolite modification with cellulose nanofiber/magnetic nanoparticles for the elimination of reactive red 198. *International Journal of Biological Macromolecules* **176**, 342–351.

Santos, S. C. R., Oliveira, Á. F. M. & Boaventura, R. A. R. 2016 Bentonitic clay as adsorbent for the decolourisation of dyehouse effluents. *Journal of Cleaner Production* **126**, 667–676.

Shoukat, R., Khan, S. J. & Jamal, Y. 2019 Hybrid anaerobic-aerobic biological treatment for real textile wastewater. *Journal of Water Process Engineering* **29**, 100804.

Singh, S., Lo, S. L., Srivastava, V. C. & Hiwarkar, A. D. 2016 Comparative study of electrochemical oxidation for dye degradation: parametric optimization and mechanism identification. *Journal of Environmental Chemical Engineering* **4** (3), 2911–2921.

Singh, R., Singh, T. S., Odiyo, J. O., Smith, J. A. & Edokpayi, J. N. 2020 Evaluation of methylene blue sorption onto low-cost biosorbents: equilibrium, kinetics, and thermodynamics. *Journal of Chemistry* **2020**. https://doi.org/10.1155/2020/8318049

Somensi, C. A., Simionatto, E. L., Bertoli, S. L., Wisniewski, A. & Radetski, C. M. 2010 Use of ozone in a pilot-scale plant for textile wastewater pre-treatment: physico-chemical efficiency, degradation by-products identification and environmental toxicity of treated wastewater. *Journal of Hazardous Materials* **175** (1–3), 235–240.

Subbaiah, V., Yarramuthi, V., Kim, Y., Min, K. & Kim, D. 2018 Ecotoxicology and environmental safety removal of anionic dyes (Reactive Black 5 and Congo Red) from aqueous solutions using banana peel powder as an adsorbent. *Ecotoxicology and Environmental Safety* **148**, 601–607.

Tayebi, H. A., Dalirandeh, Z., Shokuhi Rad, A., Mirabi, A. & Binaeian, E. 2016 Synthesis of polyaniline/Fe_3O_4 magnetic nanoparticles for removal of reactive red 198 from textile waste water: kinetic, isotherm, and thermodynamic studies. *Desalination and Water Treatment* **57** (47), 22551–22563.

Toor, M., Jin, B., Dai, S. & Vimonses, V. 2015 Activating natural bentonite as a cost-effective adsorbent for removal of Congo-red in wastewater. *Journal of Industrial and Engineering Chemistry* **21**, 653–661.

Xue, C., Chen, Q., Liu, Y. Y., Yang, Y. L., Xu, D., Xue, L. & Zhang, W. M. 2015 Acid blue 9 desalting using electrodialysis. *Journal of Membrane Science* **493**, 28–36.

Zhao, G., Zhang, H., Fan, Q., Ren, X., Li, J., Chen, Y. & Wang, X. 2010 Sorption of copper(II) onto super-adsorbent of bentonite-polyacrylamide composites. *Journal of Hazardous Materials* **173** (1–3), 661–668.

Zhirong, L., Azhar Uddin, M. & Zhanxue, S. 2011 FT-IR and XRD analysis of natural Na-bentonite and Cu(II)-loaded Na-bentonite. *Spectrochimica Acta – Part A: Molecular and Biomolecular Spectroscopy* **79** (5), 1013–1016.

Zhou, Y., Lu, J., Zhou, Y. & Liu, Y. 2019 Recent advances for dyes removal using novel adsorbents: a review. *Environmental Pollution* **252**, 352–365.

First received 27 June 2021; accepted in revised form 24 February 2022. Available online 18 March 2022